

SF3M software: 3-D photo-reconstruction for non-expert users and its application to a gully network

C. Castillo^{1,2}, M. R. James³, M. D. Redel-Macías², R. Pérez², J. A. Gómez¹.

1 Institute for Sustainable Agriculture. CSIC. Apartado 4084. 14080 Cordoba Spain.

*Corresponding author (ccastillo@ias.csic.es)

2 University of Cordoba, Dep. of Rural Engineering, Campus Rabanales, Leonardo Da Vinci Building, 14071 Cordoba, Spain.

3 Lancaster Environment Center. Lancaster University. Lancaster, UK.

Abstract

3D photo-reconstruction (PR) techniques have been successfully used to produce high resolution surface models for different applications and over different spatial scales. However, innovative approaches are required to overcome some limitations that this technique may present for field image acquisition in challenging scene geometries. Here, we evaluate SF3M, a new graphical user interface for implementing a complete PR workflow based on freely available software (including external calls to VisualSFM and CloudCompare), in combination with a low-cost survey design for the reconstruction of a several-hundred-meters-long gully network. SF3M provided a semi-automated workflow for 3D reconstruction requiring ~49 hours (of which only 17% required operator assistance) for obtaining a final gully network model of >17 million points over a gully plan area of 4,230 m². We show that a walking itinerary along the gully perimeter using two light-weight automatic cameras (1 second time-lapse mode) and a 6-m-long pole is an efficient method for 3D monitoring of gullies, at a low cost (~1,000 € budget for the field equipment) and time requirements (~90 min for image collection). A mean error of 6.9 cm at the ground control points was found, mainly due to model deformations derived from the linear geometry of the gully and residual errors in camera calibration. The straightforward image collection and processing approach can be of great benefit for non-expert users working on gully erosion assessment.

Keywords: Structure-from-motion, gully erosion, photo-reconstruction, accuracy, graphical user interface

1. Introduction

3D photo-reconstruction (PR) based on structure-from-motion (SfM) algorithms has been applied to date to a large number of geoscience applications (James and Robson, 2012; Westoby et al., 2012; Fonstad et al., 2013). Although there has been a great advance in the last years regarding imagery collection (for instance, derived from the development of UAV platforms) and image processing (commercial as well as free software), the complete photo-reconstruction (PR) and analysis workflow frequently

38 remains lengthy and not straightforward (Kaiser et al., 2014). If using freely available
39 software, it requires working on a number of different applications to cover basic image
40 pre-processing, photo-reconstruction, georeferencing and post-processing operations.
41 Commercial PR software generally has the ability to perform full PR workflows, but
42 can lack detailed processing information and can restrict user interaction with
43 intermediate and final results.

44 While recent UAV technologies have the capacity of surveying large areas of the
45 landscape (Mathews and Jensen, 2013; Mancini et al., 2013), not all stakeholders (e.g.
46 researchers, technicians and land owners) have the technical and financial resources to
47 use such sophisticated techniques. In addition, government regulations in several
48 countries are becoming increasingly stringent for UAV operations, which hampers the
49 widespread application of this tool.

50 Thus, there is still a need in developed and developing countries to implement
51 efficient terrestrial PR methodologies (in terms of budget and time requirements) for
52 scientific and technical users concerned with geomorphological processes, such as gully
53 erosion. Fonstad et al. (2013) suggested that terrestrial PR techniques could improve
54 their cost-benefit performance by using multiple operators, poles, video capture or a
55 combination of terrestrial and aerial images. New technologies (such as light-weight
56 cameras) and recent computer developments offer new opportunities to improve data
57 collection and processing. Powerful and freely available software applications have
58 been developed - e.g. VisualSFM for photo-reconstruction (Wu, 2013) or
59 CloudCompare for cloud processing (Girardeau-Montaut, 2015) among others - and are
60 being constantly improved through the valuable effort of their developers and users'
61 feedback.

62 3D PR has been used for gully erosion assessment at the gully reach or headcut
63 scale (Castillo et al., 2012a; Kaiser et al., 2014; Gómez Gutiérrez et al., 2014) and
64 ephemeral gullies (Castillo et al., 2014), usually not more than over a few meters extent.
65 However, the fully characterization of gully erosion requires the assessment of entire
66 gully networks to understand their geometry and dynamics and this brings several
67 challenges for terrestrial PR: 1) morphological complexity: gullies comprise long
68 networks of varying size along their length; 2) valley location: gullies are deep trenches
69 that do not facilitate easy all round image collection, hampering multiple convergent
70 perspectives; 3) linearity: gullies present very high length/width ratios making the
71 photo-reconstruction models more vulnerable to systematic errors.

72 As an effort to facilitate the use of freely available PR software for demanding
73 gully erosion applications, here we develop a combination of a rapid survey method and
74 SF3M, a workflow software tool for efficient processing of accurate 3D models of gully
75 networks at a reduced cost. For this purpose, 1) we present SF3M, a new graphical user
76 interface to guide PR workflow carried out with existing freely available software; 2)
77 we describe a field methodology for the rapid assessment of gully networks; and 3) we

78 evaluate their performance and the 3D model accuracy with a study case of gully
79 erosion in the Campiña landscape.

80 **2. Material and Methods**

81 **2.1. SF3M: a GUI for efficient photo-reconstruction**

82 SF3M v1.0 has been devised as a freely available tool for semi-automated 3D
83 PR to offer a complete workflow from the image set to the 3D model. SF3M v1.0 is
84 written in Matlab[®] (Mathworks, Natick, MA, USA) and comprises algorithms
85 developed by the authors of this manuscript, a number of previous scripts written by
86 other authors (Table 1) as well as external calls to free software such as VisualSFM
87 (Wu, 2013; Wu, 2015) and CloudCompare (Girardeau-Montaut, 2015). SF3M takes
88 advantage of the command line possibilities already present in these external
89 applications to perform key operations, such as photo-reconstruction (including SIFT
90 features detection, bundle adjustment, sparse and dense reconstruction inside the
91 VisualSFM package) and point cloud processing (i.e. point density, filtering and
92 merging operations in CloudCompare).

93 The GUI is organized in three windows: main, image and display window (Fig.
94 1). The main window allows the user to define the operations to be performed. The
95 image window can be used to visualize a photograph, and to enter and delete ground
96 control point (GCP) observations. The display window gives information on the stage in
97 process, time left to finish and main results.

98 SF3M v1.0 use follows a sequential process including pre-preprocessing,
99 reconstruction, georeferencing and post-processing stages. All the command options are
100 displayed in the main window so that the user can enter the processing options in
101 advance and leave the application running automatically. This design is intended to
102 keep the GUI operation as simple as possible, facilitating its use for non-trained users.

103 The main features of the SF3M are outlined in Table 1. For a more detailed
104 description of SF3M v1.0 functionalities, the SF3M executable and instructions are
105 available at SF3Mapp.csic.es.

106

107 **2.2. Field methodology for rapid gully network assessment**

108 We designed a methodology of field image collection for rapid gully erosion
109 reconstruction based on four principles:

110 1- automated image collection from a pole to capture high centre-perspectives of
111 the gully from its perimeter

112 2- near-simultaneous capture of two perspectives (two cameras needed on the
113 pole), with one vertical and the other inclined, to: 1) maximise the probability of
114 successful image matching between photographs taken from different sides of the gully,

115 in order to achieve a single 3D model; 2) ensure a convergent imaging geometry to help
116 minimise systematic reconstruction errors and model distortion.

117 3- image capture from only one walking itinerary along the entire gully
118 perimeter

119 4- use of low-cost devices and materials for image collection

120 As an application of the SF3M processing method, a gully erosion survey was
121 conducted in a gully network close to the city of Córdoba (Spain) covered with field
122 crops on vertic soils with marls as parent material (37°50'27.4"N, 4°47'59.7"W, Fig. 2).
123 The gully was 510 m long in its main channel and as 11 m wide and 3 m deep in its
124 larger cross sections. Each of the three gully branches were taken as separate photo-
125 reconstruction units in the field and processing stages. The gully network was selected
126 for its convenient location near to Córdoba city as well as for having been filled in
127 during 2008, which provides a baseline to estimate recent gully erosion.

128 In this study, two GoPro Hero3+ cameras equipped with non-fisheye lenses, i.e.
129 4.14 mm focal length, f/3.0 aperture and 5.4 mm focal length, f/2.8 aperture,
130 respectively (Peau Productions, CA, USA, <http://www.peauproductions.com/store/>).
131 The cameras were mounted on a 6 m-long pole (made from a 9 m-long carbon-fibre
132 telescopic fishing rod) to gain height to capture the gully dimensions from a centre
133 position in time lapse capture mode (1 second interval). To reduce camera vibrations,
134 the unused three meters of the telescopic 9-m-long fishing rod were secured with plastic
135 cable ties at the end of the 6 m pole.

136 Both cameras were fixed to the pole end adjacent to each other and held in a
137 horizontal position with the help of plastic wedges and cable ties. One camera looked
138 down in a roughly nadir perspective (closest to the pole end for a higher elevation to
139 compensate for the less deep perspective) and the other was inclined to around 10°. This
140 camera arrangement was intended to: a) obtain a high overlap between images taken
141 with both cameras; 2) ensure the connectivity of the whole image set obtained from
142 different sides of the gully: the two nadir image sets (up- and downwards itineraries)
143 will serve as connectors and the two tilted sets will provide image convergence. Both
144 aspects would be helpful to obtain one single 3-D model with geometric consistency.
145 The typical overlap derived from this camera setting, the walking speed and the time-
146 lapse interval was around 90% for successive images taken from the same camera. As
147 for the overlap between different camera images, the tilted images encompassed totally
148 the scene captured by the nadir camera due to its higher position and inclined
149 orientation (Fig. 3a and 3b).

150 An uninterrupted itinerary along the gully perimeter was followed at a slow
151 walking speed, starting from one point and ending on the opposite side of each gully
152 branch (Fig. 3c). Forty five targets, hereafter called ground control points (GCPs), of
153 20x20 cm dimensions in two colours (pink for even numbers and yellow for odd
154 numbers). This colour symbology was meant to differentiate georeferencing GCPs

155 (even numbers) and error-checking GCPs (odd numbers) to facilitate the operator the
156 deployment of targets in the field.

157

158 **2.3. Processing methodology in SF3M**

159 The key features of the processing workflow followed using SF3M v1.0 are
160 listed below:

161 1. Simplicity in the design and operation, with only one GUI window to define the array
162 of algorithms to run. The typical operation for a project reconstruction would include
163 five sequential steps: a) pre-processing to prepare the image set (automated); b) project
164 definition, to check the image connectivity and the number of subprojects to process
165 (semi-automated); c) photo-reconstruction (automated); d) georeferencing (semi-
166 automated); e) post-processing (semi-automated). Within each of these steps for a PR
167 project, several options can be selected for successive processing, e.g. blurry images
168 detection + image undistortion or green index filter + density filter + Merge + DEM +
169 SfM accuracy. In addition, if the batch mode is activated, the selected operations can be
170 performed over different PR projects.

171 2. Camera calibration: SF3M does not perform camera calibration. However, SF3M
172 settings include the option to enter camera parameters (focal length and principal point)
173 for use with undistorted images and the fixed camera calibration mode in VisualSfM.
174 In this work, we could not take advantage of this option because VisualSfM does not
175 allow simultaneous use of more than one camera in this mode. Therefore, the internal
176 camera parameters were estimated automatically during the bundle adjustment in
177 VisualSfM.

178 Furthermore, SF3M allows the user to undistort images if camera calibration data is
179 available from the Matlab Calibration Toolbox (Bouguet, 2014). For our study, both
180 cameras were calibrated using this toolbox and all images were then undistorted keeping
181 the VisualSfM ‘determine radial distortion option’ disabled.

182 3. Pair preselection: a first fast run of VisualSfM is performed to identify the significant
183 matches between image pairs (pairs with inlier matches) by comparing all the possible
184 pair combinations, but using only a relatively small number of features from each image
185 for speed. SF3M sets a limit of 1,200 features to use in the VisualSfM settings (the
186 default value is 8,192) for the project connectivity analysis. This value has proved to be
187 sufficiently large to accurately capture the image connection, but at a minimum
188 processing cost.

189 As a result of this analysis, a list of connected image pairs is generated, which
190 will be the input to the final matching stage. This list includes generally much fewer
191 image pairs than all the possible combinations among the pictures. The number of the
192 possible combinations (and consequently, processing time) follows a square power law
193 with the number of pictures, while normally the image connection is highly linear (only

194 pictures in the neighbourhood share common features). This results in a significant
195 reduction on the match processing duration, one of the more time consuming stages.

196 4. Subproject delineation: In SF3M the project connectivity analysis not only checks for
197 the production of a single model and generates an optimal pair list but also provides the
198 approximate locations of cameras with GCPs (provided that GCP observations have
199 been entered by the user in the image window and the search GCPs algorithm
200 performed). This option allows the delineation of subprojects, which are reconstructed
201 separately, by selecting the cameras to be included in the analysis with a polygon
202 drawing tool. Overlapping areas between subprojects are recommended to reduce the
203 errors in the merging process. This tool is advantageous for field surveys where images
204 of the same areas are taken at different times (e.g. in a gully, the upstream and
205 downstream walks on different sides of the same gully region) and to minimise the
206 effects of systematic errors in large image sets.

207 5. Photo-reconstruction: in SF3M v1.0 the photo-reconstruction stage is carried out
208 through a system call to VisualSFM using command line syntax to drive automated
209 processing. The main VisualSFM commands used in our utility are: extracting SIFT
210 features, image matching, exporting match matrix, bundle adjustment and dense
211 reconstruction (multi-view stereo PMVS2 software, Furukawa and Ponce, 2010).

212 6. Georeferencing: We followed a similar approach to that developed in SfM_georef
213 (James and Robson, 2012). The GCP observations are entered manually in the image
214 window. The GCP table in the main window provides information on the number of
215 observations per GCP, the image errors (in pixels) and the absolute errors (m). The tool
216 gives the option of selecting which GCP are to be used for georeferencing (georef
217 GCPs) and which other are used to evaluate errors (control GCPs).

218 7. Dense cloud filtering: SF3M includes two optional filters to be applied to the dense
219 point clouds. The green index filter removes those points with a green index above the
220 threshold selected by the user, for instance, green parts of vegetation standing at the
221 banks or gully bottom. The green index is calculated using $GI = 2g - b - r$, where r, b and g
222 stands for the pixel value of each of the colour bands in the RGB image (Meyer and
223 Neto, 2008). The density filter is intended to remove those points with a low point
224 density in their neighbourhood, typically related to lower accuracies. It is also helpful to
225 remove inaccurate points in overlapping areas shared by two dense point clouds which
226 may reduce the accuracy of pre-existent more accurate points. The density filter is
227 performed automatically through command line calls to two CloudCompare algorithms:
228 density calculation and filter by point value.

229 8. Merging dense point clouds: SF3M automatically merges all the dense point clouds
230 belonging to a subproject using CloudCompare in command line. If subproject
231 definition is not carried out, the resulting merged file is the final dense point cloud. For
232 multiple subprojects, to obtain the final point cloud, the intermediate subproject clouds
233 need to be merged manually by the user (step 9).

234 9. Point cloud editing: two manual operations were performed fully inside
235 CloudCompare: subproject and project merging, and non-green vegetation filtering.

236 The merging procedure involves the following algorithms: a) distance cloud-to-cloud of
237 adjacent clouds to determine the specific area inside the overlapping region with
238 minimal errors; b) cropping both point clouds along this area of minimal error to
239 remove the overlapping ; c) merging the point clouds.

240 To filter non-green vegetation (long-standing greyish prickly weeds, in our case) the
241 point classification algorithm CANUPO (Brodu and Lague, 2012) was used, through its
242 inclusion as a ready-to-use script in CloudCompare. CANUPO performs a point
243 classification into two groups (in this example, weeds and soil) after a training stage
244 carried out by the user.

245 10. Results: SF3M provides the DEM (average of the z values of points included in a
246 cell of a size defined by the user), a point density map (points/m²) and an ‘SfM
247 precision’ map. A decimation factor can be included to speed up the processing, i.e. a
248 factor of ten would include only a tenth of the points in a cell for the computations, for
249 processing large or particularly dense point clouds. We use the term ‘SfM precision’ to
250 describe local uncertainties in the sparse point cloud. For each point, the local
251 uncertainty is approximated by considering (a) the camera’s focal length, (b) the
252 camera-to-point distance in world coordinates, and (c) the maximum image error, where
253 image error is defined as the image distance between an identified feature position and
254 the projection of the associated 3D point in that image. This SfM error is estimated with
255 the following expression:

$$\text{SfM precision (mm)} = \frac{\text{image_error(pixels)}}{\text{focal_length(pixels)}} \cdot \text{distance_point2camera(mm)}$$

256 [1]

257 Typically, the local precision is higher than the final accuracy measured by
258 ground control reference, since it does not include any wider geometric distortion that
259 may exist across a model. Nevertheless, it provides a useful quantification of photo-
260 reconstruction error on a local basis.

261 Finally, SF3M v1.0 saves relevant outputs in the main folder for further edition
262 by the user in csv, txt or ascii formats such as matching features, transformation
263 matrices, DEM or point density map, among others. Figure 4 shows the SF3M
264 workflow with indication of the command options to be selected in the main window.

265

266 3. Results

267 3.1. Field method performance

268 Table 2 shows the field and processing time requirements for this study. A total
269 of 6650 images were taken in the field for the entire gully network at a rate of one
270 picture per second and camera. Approximately 90 min of effective labour (travel to
271 study area, pole preparation and GPS base stationing not considered) were necessary for
272 the field survey. Image collection and GCP operations (deployment and measurement)
273 had similar time requirements, ~90 min each. Two operators participated in the survey,
274 one for the image capture and the other for GCP measurement, working simultaneously
275 for efficiency purposes.

276 If no georeferencing had been necessary (for instance, if there is no need of
277 several time series comparison) a much faster approach for scaling and orientation
278 might be followed, using levelled objects of known size, as in previous works (Castillo
279 et al., 2014; Kaiser et al., 2014). In highly linear models such as the gully network,
280 simple procedures (e.g. a carefully levelled several-meters-long thin rope commonly
281 used in construction works) are applicable for later scaling and orientation using a point
282 cloud editing software.

283 Over recently ploughed gully margins, a walking speed of ~1.5 km/h
284 (approximately a third of normal speed) was necessary to avoid undesired movement in
285 the camera and blurred images. Despite the lightness of the selected materials (pole and
286 cameras) a short break in the image collection was made after completing each of the
287 gully branches to avoid operator fatigue. The camera height (~5 m for the inclined 6 m-
288 long pole) was enough to capture the gully dimensions in its larger cross section (11 m).
289 This gully width seems the maximum achievable for the present image collection
290 design.

291

292 **3.2. SF3M processing performance**

293 With images taken at 1 second intervals, the image set could be reduced by a
294 factor of two due to repetition within the pictures. The remaining 3,275 images were
295 automatically analysed for blur and 180 images with a blur index greater than two
296 standard deviations above the mean value, were discarded (Fig. 5a).

297 As expected, the project connectivity showed a multiple-matching pattern
298 reflecting the nadir and tilted camera angles and downstream and upstream walking
299 directions (Fig. 5b). The match matrix diagonal corresponds to the connection between
300 consecutive images; additional lines parallel or perpendicular to the diagonal reflect
301 connectivity between upstream and downstream image groups from the same or
302 different cameras.

303 The gully network was processed as three different PR projects (reflecting the
304 number of gully branches) which were then merged in a single point cloud. For the
305 computer used in this study (intel Core i7 2Ghz with 4 cores, 8GB RAM), a total of
306 2,960 minutes were necessary to process the entire gully network, i.e. ~ 49 hours, of

307 which 17% required operator assistance and 83% only computer time. Photo-
308 reconstruction (54.5% of the total time) and picture undistortion (15.2 %) were the two
309 most time-consuming stages.

310 All the processing steps were performed using SF3M v1.0 except for those
311 specified in the methods section which required point cloud editing in CloudCompare:
312 1) subproject merging for the chunks reconstructed separately inside a gully branch to
313 reduce model deformation; 2) project merging for the three gully branches; 3) non-green
314 vegetation filter using CANUPO. Regarding the vegetation filtering, firstly the
315 automated green index filter was applied inside SF3M resulting in a 3.5 % of the total
316 points in the model removed corresponding to small green weeds (Fig. 6a). The second
317 main type of vegetation in the gully was a tall-standing greyish weed, which was
318 filtered using CANUPO. The points filtered as this last type of vegetation amounted to
319 4.1% of the total, although its detrimental effects on the model were significant at some
320 gully bottom areas (Fig. 6b).

321 The final gully model had >17 million points over a plan area of 4,230 m²,
322 making a point density average of 4,020 points/m² (Fig. 6c), or approximately 1 point
323 every 2 cm², which was sufficient for the 3D modelling purposes at this scale. A higher
324 point density (roughly twice the number of points) could have been achieved by
325 selecting the maximum density level in the pmvs2 algorithm at the cost of longer
326 processing time in the dense reconstruction stage (approximately by a factor of 5). In
327 many applications, higher densities might be impractical and not required for DEM
328 construction. The final photo-reconstruction percentage (the cells with elevation values
329 to total cells ratio) for the 0.25 m DEM was 74.25 %, due to the abundant vegetation
330 occlusion at the gully bottom in certain areas.

331

332 **3.3. 3-D Model accuracy**

333 For the present application, an average GCP error of 6.9 cm was found (Fig. 7a).
334 The GCP error is defined as the distance in world coordinates between each GCP centre
335 location in the final georeferenced point cloud and the GCP centre coordinates
336 measured by dGPS in the field. When compared with the average local SfM precision
337 value (Eq. 1), the average GCP error was significantly larger, i.e. 6.9 cm against 2.5 cm
338 (Fig. 7b).

339 There are a variety of sources of error as a consequence of the inexpensive and
340 rapid survey methodology selected in this study such as low-quality camera lenses,
341 uncertainty in the internal camera parameters of the GoPro camera models, reduced
342 number of perspectives from images with only two main angles and the low number of
343 pictures per spatial unit. All these factors may contribute to error in the 3D model both
344 on the local scale (i.e. in the form of uncertainties in the point position) and the model
345 scale (geometrical deformations due to systematic errors accumulating over the model
346 extent).

347 The discrepancy between the GCP error and the estimated SfM precision can be
348 explained mainly as the result of the model deformation at the several-tens-of-meter
349 scale, and is likely to reflect residual error in the camera calibrations (James & Robson,
350 2014). This deformation is visualized as an apparent dome effect at both extremes of
351 each dense point cloud, with increasing error for larger distances from the point cloud
352 centroid. Although the image collection was designed to minimise this effect by
353 specifically including inclined images, doming effects remain noticeable.

354 In this study, the most successful strategy to mitigate the model deformation was
355 to divide the photo-reconstruction project in different subprojects for separate
356 reconstruction using the subproject tool in SF3M. The length of each subproject was
357 defined by the condition of including at least 4 GCPs. Since a total of 45 GCPs were
358 deployed in the field, an average length of ~50 m per subproject was obtained. This
359 approach was advantageous in terms of overall accuracy but implied an additional
360 processing time for manually stitching and merging the 17 subprojects in
361 CloudCompare by determining the area of minimal error between adjacent point clouds.

362 If the subproject definition strategy would not be applied, for instance by
363 reconstructing a several-hundred-meters gully reach in one project, the deformation
364 errors would have been in the order of several tens of centimeters. Similarly, James and
365 Robson (2014) found doming deformations of ~0.2 m over horizontal distances of ~100
366 m for simulations representative of UAV flights. Their recommendations on using fixed
367 calibration to avoid doming errors could not be followed because VisualSfM does not
368 include a fixed calibration option for multiple cameras.

369 When compared with previous studies on gully erosion assessment through SfM
370 photo-reconstruction (Castillo et al., 2012a; Gómez-Gutiérrez et al., 2014; Kaiser et al.,
371 2014; Castillo et al., 2014) in terms of unitary efficiency (field effort per meter of
372 gully), this work showed larger errors (roughly 2 times the average errors in those
373 studies) but at a lower survey intensity (images per meter of gully) and at one order of
374 magnitude lower time requirements (Table 3).

375

376 **3.4. Gully erosion estimate**

377 The resulting DEM was used to estimate the gully volume and a gully erosion
378 estimate, taking the 2008 filled situation as a reference. The volume was determined
379 using the Cut and Fill algorithms in ArcGis™ 9.3 (ESRI Inc., Redlands, CA, USA). The
380 gully limits were delineated manually by interpreting the DEM and slope maps since, in
381 some areas, the gully rims were not well represented in the dense point cloud and
382 automated methods were not fully applicable.

383 A total gully volume of 3,484 m³ was obtained for a drainage area of 10.9 has at
384 the gully network outlet. We assumed that the gully was filled in the summer of 2008
385 (common period for this operation in the Campiña landscape) since the

386 orthophotography (april 2009) shows the gully already filled (Fig. 8). Also, due to the
387 similarity in the gully network of 2011 and 2014 (present study), there is no evidence of
388 further major filling operations between these dates.

389 Considering a bulk soil density of 1.5 Mg/ m^3 , typical of vertic soils in our
390 conditions and a time span of six years, an average gully erosion estimate of 79.5
391 Mg/ha-year was calculated. Most likely, the peak of gully erosion took place during the
392 2009 and 2010, a wet period with annual rainfalls exceeding 1000 mm in the area (425
393 mm in one month during December 2009-january 2010 and 350 mm during December
394 2010). These wet years were preceded and followed by seasons closer to the average
395 (650 mm per year). This high value of mean gully erosion is in agreement with previous
396 assessments for similar conditions over the same period (Castillo et al., 2012b).

397

398 **4. Conclusions**

399 3D photo-reconstruction techniques based on SfM algorithms have already
400 demonstrated their capability for producing accurate 3D models in a range of
401 geoscience applications. Nevertheless, research is still needed to improve efficiency in a
402 number of challenging situations and their ease of use for workers not necessarily
403 skilled in photogrammetric applications. SF3M v1.0 proved to be an efficient and
404 flexible tool for 3D photo-reconstruction in these regards, considering its simplicity and
405 complete workflow.

406 To the author's knowledge, this is the first time an entire several-hundred-
407 meters-long gully network has been surveyed by terrestrial photo-reconstruction. This
408 was carried out using inexpensive means (around 1,000 € budget for the field
409 equipment), little manpower (a minimum of one operator is required), in a short time
410 span and has achieved moderate accuracies. Therefore, the survey design and
411 processing methodology included in this study is a promising tool for gully erosion
412 evaluation in scenarios with demanding budget and time constraints and reduced
413 operator expertise. Moreover, SF3M provides a means for easy and fast 3-D photo-
414 reconstruction in other geomorphological applications beyond gully erosion assessment.
415 Future versions of SF3M will try to include new tools including improved GCPs
416 detection and post-processing algorithms such as topographic analysis of the resulting
417 DEM along with further improvement on the interface usability or on other aspects that
418 might be suggested from users' feedback.

419

420 **5. Acknowledgements**

421 This study was supported by Projects P08-AGR-03925 (Andalusian
422 Government) and AGL2009-12936-C03-01 (Spanish Ministry of Science and
423 Innovation), AGL2012-40128-C03-01 (Spanish Ministry of Economy and
424 Competitiveness), RESEL (Spanish Ministry for Environment and Rural and Marine

425 Affairs) and FEDER funds. This support is gratefully acknowledged. The authors would
426 like to thank José Manuel Cabezas for his contribution in the gully survey. We also
427 express our gratitude to all developers of freely available software for their generous
428 contributions, especially to Changchang Wu and Daniel Girardeau-Montaut.

429

430 **6. References**

431 Boughet, J.: Undistortion script (Matlab Camera Calibration Toolbox).
432 http://www.vision.caltech.edu/boughetj/calib_doc/ (last access December 2014).

433 Brodu, N., and Lague, D.: Terrestrial lidar data classification of complex natural scenes
434 using a multi-scale dimensionality criteria : applications in geomorphology. *Journal of*
435 *Photogrammetry and Remote Sensing* 68: 121-134. (IF 2.90), 2012.

436 Castillo, C., Pérez, R., James, M.R., Quinton, J.N., Taguas, E.V., and Gómez, J.A.:
437 Comparing the Accuracy of Several Field Methods for Measuring Gully Erosion. *Soil*
438 *Sci. Soc. Am. J.* 76, 1319–1332. doi:10.2136/sssaj2011.0390, 2012a.

439

440 Castillo, C., Pérez, R., Mora., J., Gómez, J.A.: Quantification of gully erosion in a
441 cultivated area in Southern Spain under high rainfall conditions. *Geophysical research*
442 *abstracts*, 14, EGU 2012-10976, 2012b.

443

444 Castillo, C., Taguas, E.V., Zarco-Tejada, P., James, M.R., and Gómez, J.A.: The
445 normalized topographic method: an automated procedure for gully mapping using GIS.
446 *Earth Surf. Process. Landf.* 39, 2002–2015. doi:10.1002/esp.3595, 2014.

447

448 Castillo, C., Rodríguez, A., Giráldez, J.V., and J.A. Gómez: Mejora de la evaluación de
449 la erosión por flujo concentrado en taludes de carreteras sobre diferentes materiales en
450 Andalucía mediante foto-reconstrucción., *Avances de la geomorfología en España*
451 *2012-2014*, 176-179, 2014.

452

453 Fonstad, M.A., Dietrich, J.T., Courville, B.C., Jensen, J.L., and Carbonneau, P.E.:
454 Topographic structure from motion: a new development in photogrammetric
455 measurement. *Earth Surf. Process. Landf.* 38, 421–430. doi:10.1002/esp.3366, 2013.

456 Furukawa, Y., and Ponce, J.: Accurate, dense, and robust multiview stereopsis. *IEEE*
457 *Trans. Pattern Anal. Mach. Intell.* 32(8):1362–1376. doi:10.1109/TPAMI.2009.161,
458 2010.

459 Girardeau-Montaut, D.: CloudCompare: 3D point cloud and mesh processing software.
460 <http://www.danielgm.net/cc/> (last Access, 20 March 2015).

461

462 Gómez-Gutiérrez, A., Schnabel, S., Berenguer-Sempere, F., Lavado-Contador, F., and
463 Rubio-Delgado, J.: Using 3D photo-reconstruction methods to estimate gully headcut
464 erosion. *Catena* 120, 91–101. doi:10.1016/j.catena.2014.04.004, 2014.

465

466 James, M.R., and Robson, S.: Straightforward reconstruction of 3D surfaces and
467 topography with a camera: Accuracy and geoscience application. *J. Geophys. Res.-*
468 *Earth Surf.* 117, F03017. doi:10.1029/2011JF002289, 2012.

469

470 James, M.R., and Robson, S.: Mitigating systematic error in topographic models derived
471 from UAV and ground-based image networks. *Earth Surf. Process. Landf.* 39, 1413–
472 1420. doi:10.1002/esp.3609, 2014.

473

474 Junta de Andalucía, Consejería de Medio Ambiente y Ordenación del Territorio:
475 [http://www.juntadeandalucia.es/medioambiente/site/rediam/menuitem.aedc2250f6db83](http://www.juntadeandalucia.es/medioambiente/site/rediam/menuitem.aedc2250f6db83cf8ca78ca731525ea0/?vgnnextoid=0863d61d8470f210VgnVCM2000000624e50aRCRD&lr=lang_es)
476 [cf8ca78ca731525ea0/?vgnnextoid=0863d61d8470f210VgnVCM2000000624e50aRCRD](http://www.juntadeandalucia.es/medioambiente/site/rediam/menuitem.aedc2250f6db83cf8ca78ca731525ea0/?vgnnextoid=0863d61d8470f210VgnVCM2000000624e50aRCRD&lr=lang_es)
477 [&lr=lang_es](http://www.juntadeandalucia.es/medioambiente/site/rediam/menuitem.aedc2250f6db83cf8ca78ca731525ea0/?vgnnextoid=0863d61d8470f210VgnVCM2000000624e50aRCRD&lr=lang_es) (last access 20 March 2015).

478

479 Kaiser, A., Neugirg, F., Rock, G., Mueller, C., Haas, F., Ries, J., and Schmidt, J.: Small-
480 Scale Surface Reconstruction and Volume Calculation of Soil Erosion in Complex
481 Moroccan Gully Morphology Using Structure from Motion. *Remote Sensing* 6, 7050–
482 7080. doi:10.3390/rs6087050, 2014.

483

484 Mancini, F., Dubbini, M., Gattelli, M., Stecchi, F., Fabbri, S., and Gabbianelli, G.:
485 Using Unmanned Aerial Vehicles (UAV) for High-Resolution Reconstruction of
486 Topography: The Structure from Motion Approach on Coastal Environments. *Remote*
487 *Sens.* 5, 6880–6898. doi:10.3390/rs5126880, 2013.

488

489 Marziliano, P., Dufaux, F., Winkler, S., Ebrahimi, T.: Perceptual blur and ringing
490 metrics: application to JPEG2000. *Signal Process.-Image Commun.* 19, 163–172.
491 doi:10.1016/j.image.2003.08.003, 2004.

492

493 Mathews, A.J., and Jensen, J.L.R.: Visualizing and Quantifying Vineyard Canopy LAI
494 Using an Unmanned Aerial Vehicle (UAV) Collected High Density Structure from
495 Motion Point Cloud. *Remote Sens.* 5, 2164–2183. doi:10.3390/rs5052164, 2013.

496

497 Meyer, G.E., and Neto, J.C.: Verification of color vegetation indices for automated crop
498 imaging applications. *Comput. Electron. Agric.* 63, 282–293.
499 doi:10.1016/j.compag.2008.03.009, 2008.

500

501 Naccari, M.: Blur_metric script. <https://sites.google.com/site/matteonaccari/software>,
502 2011 (last access November 2014).

503

504 Stevens, A.: Arcgridwrite matlab script. [http://www.mathworks.com/](http://www.mathworks.com/matlabcentral/fileexchange/16176-arcgridwrite/content/arcgridwrite.m)
505 [matlabcentral/fileexchange/16176-arcgridwrite/content/arcgridwrite.m](http://www.mathworks.com/matlabcentral/fileexchange/16176-arcgridwrite/content/arcgridwrite.m), 2007 (last
506 access november 2014).

507

508 Westoby, M.J., Brasington, J., Glasser, N.F., Hambrey, M.J., and Reynolds, J.M.:
509 “Structure-from-Motion” photogrammetry: A low-cost, effective tool for geoscience
510 applications. *Geomorphology* 179, 300–314. doi:10.1016/j.geomorph.2012.08.021,
511 2012.

512

513 Wu, C.: Towards linear-time incremental structure from motion. *International*
514 *Conference on 3D vision publication (3DV Conference, Seattle, WA, USA, June 2013)*,
515 127-134, 2013.

516
517 Wu, C.: VisualSFM : A Visual Structure from Motion System. <http://ccwu.me/vsfm/> ,
518 2015 (last access, 3 March 2015).
519

520

521

522

523

524

525

526

527

528

529

530

531

532

533

534

535

536

537

538

539

540

541

542

543

544 Table 1. SF3M v1.0 features showing the aim of each stage, and software used.

SF3M FEATURES	Purpose	External software	
		Tool	Type
Preprocessing			
Reducing the number of pictures	Decrease the total number of images	----	----
Detecting blurry images	Discard blurry images.	Blur_metric ¹	Matlab script
Renaming pictures	Change the initial character string of the image name	----	----
Picture undistortion	Undistortion of pictures	Undistort ²	Matlab script
Project			
Project connectivity	Check if the image set produces a single model	VisualSFM ³	3D Photo-reconstruction
Search GCPs in pictures	Identify GCP candidate by colour in images to facilitate GCP observations input	----	----
Preliminary camera location with GCPs	Approximated location of cameras to facilitate subproject definition	----	----
Subproject definition	Generate different separate subsets for PR	----	----
Photo-reconstruction			
Sparse and dense reconstruction	3D model in relative SfM coordinates	VisualSFM ³	3D Photo-reconstruction
Georeferencing			
GCP observations input and deletion	Managment of GCP observations by visual identification on image window	----	----
Highlight of images with detected GCPs	Facilitates GCP observations input on image window	----	----
Highlight of images with observation and GCP number	Facilitates GCP observations input and removal	----	----
Georef GPC and control GCP	Setting GCP reference and control errors	----	----
Calculation of image errors	Errors in image measurements (collinearity equations)	----	----
Transformation matrix, georef and control errors	Absolute error determination	----	----
Application of transformation matrix for each option file	Transforming the dense point clouds from camera to world coordinates	----	----
Post-processing			
Green index filter	Removing points candidates to vegetation in dense clouds	----	----
Density filter	Removing points with low point density in its neighborhood	CloudCompare ⁴	Point cloud editing
Merge dense	Merge dense point clouds for subprojects	CloudCompare ⁴	Point cloud editing
Results			
DEM (m)	DEM in asc format as an elevation average in a cell	arcgridwrite ⁵	Matlab script
Point density (points/m2)	Point density map	----	----
SfM precision (mm)	SfM error in sparse point cloud (Eq. 1)	----	----

¹ Naccari, 2011. Matlab script for image blur metrics based of the blur index developed by Marziliano et al. (2004); ²Boughet, 2014; ³Wu, 2013; ⁴Girardeau-Monteaut, 2015; ⁵Stevens, 2007

545 Table 2. Field and processing time requirements for the entire gully network. Main
 546 results and type of operation are included.

SF3M operation	Operation	Result	Time (min)
Field survey			170
Image collection	Manual	6550 images	80
GCP deployment and GCP measurement	Manual	45 GCPs measured	90
Preprocessing			487
Reducing the number of pictures	Automated	3275 images discarded	5
Detecting blurry images (blur index threshold = 2)	Automated	180 images discarded	32
Picture undistortion	Automated	3095 images undistorted	450
Project analysis			263
Project connectivity	Automated	Matrix of matches	55
Search GCPs in pictures	Automated	GCP identified in image window	48
Manual input GCP observations	Manual	300 observations from 45 GCP	120
Manual subproject delineation	Manual	17 subprojects	40
Photo-reconstruction			1,615
Sparse reconstruction	Automated	17 sparse clouds	765
Dense reconstruction (medium level)	Automated	119 dense files	850
Georeferencing			60
Calculation of image errors	Automated	Image errors	--
Calculation of transformation matrix, georef and control errors	Automated	Georef errors	--
Application of transformation matrix for each option file	Automated	119 georeferred dense clouds	60
Post-processing			318
Green index filter (green index threshold = 30)	Automated	Average of 3.5 % points removed	68
Density filter	Automated	Average of 1.2 % points removed	55
Merge dense clouds	Automated	17 merged clouds	25
Merge subprojects and projects	Manual	1 final point cloud	110
Remove non-green vegetation (Canupo)	Manual	Average of 4.1 % points removed	60
Results			47
DEM (m) and Point density (points/m ²)	Automated	DEM and point density ascii file	25
SfM precision (mm)	Automated	SfM accuracy map for a project	22
			2,960

547

548

549

550 Table 3. Comparison between the survey intensity (number of pictures per meter of
 551 gully) and time requirements (image collection time per meter of gully) for different
 552 gully erosion studies using SfM photo-reconstruction including the present study.

553

Author	Year	Gully feature	Length (m)	Average Errors (m)	Number of pictures	Time for image collection (min)	Survey intensity (pictures/m)	Time requirements (min/m)
Castillo et al.	2012a	Reach	7.1	0.025	191	10	26.9	1.4
Gómez-Gutiérrez et al.	2014	Headcut	6	0.048	64	NA	10.7	NA
Kaiser et al.	2014	Headcut	4	--	257	30	64.3	7.5
Castillo et al.	2014	Ephemeral	30	0.036	515	90	17.2	3.0
Present study	2015	Network	750	0.069	3,275	80	4.4	0.1

554

555

556

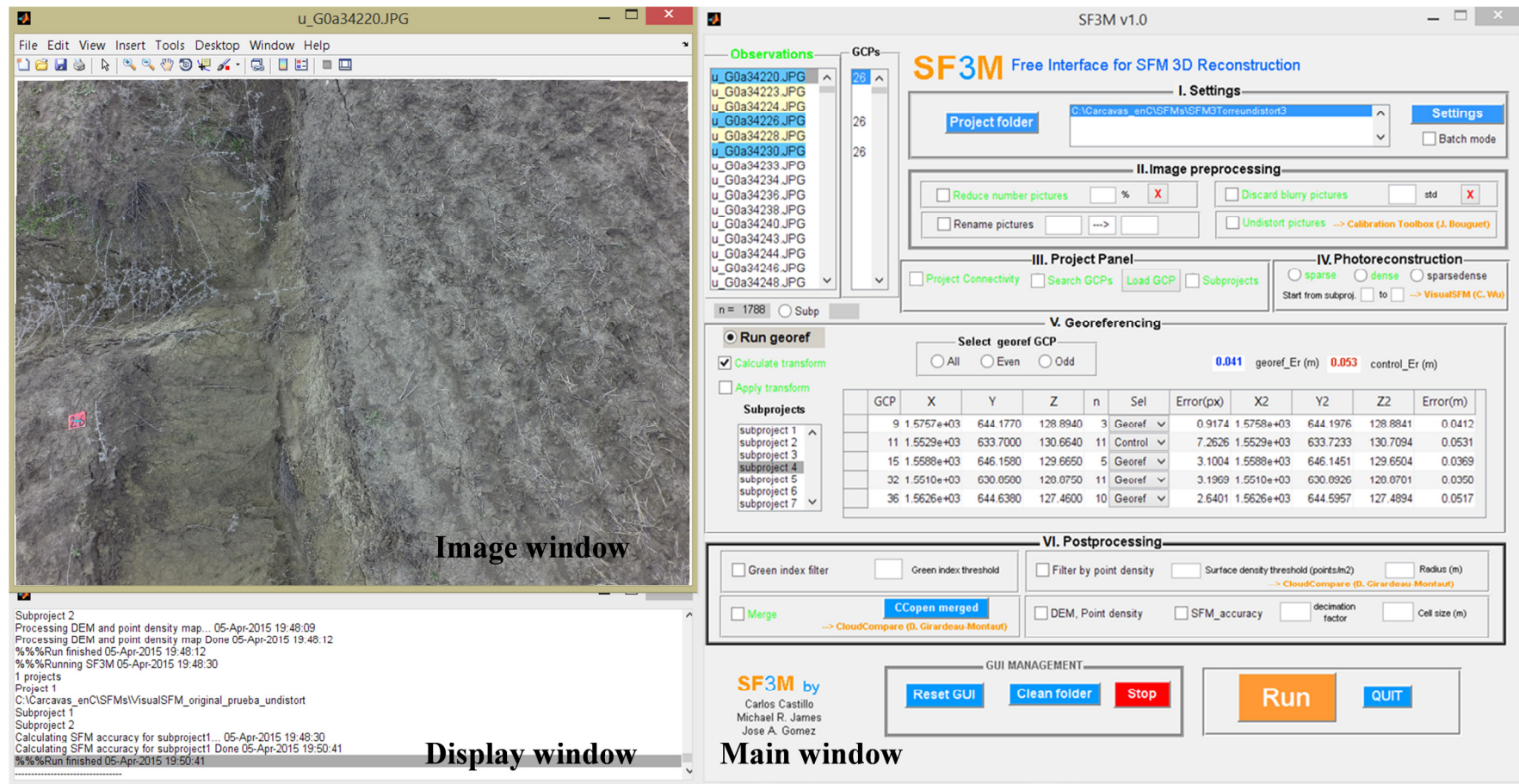
557

558

559

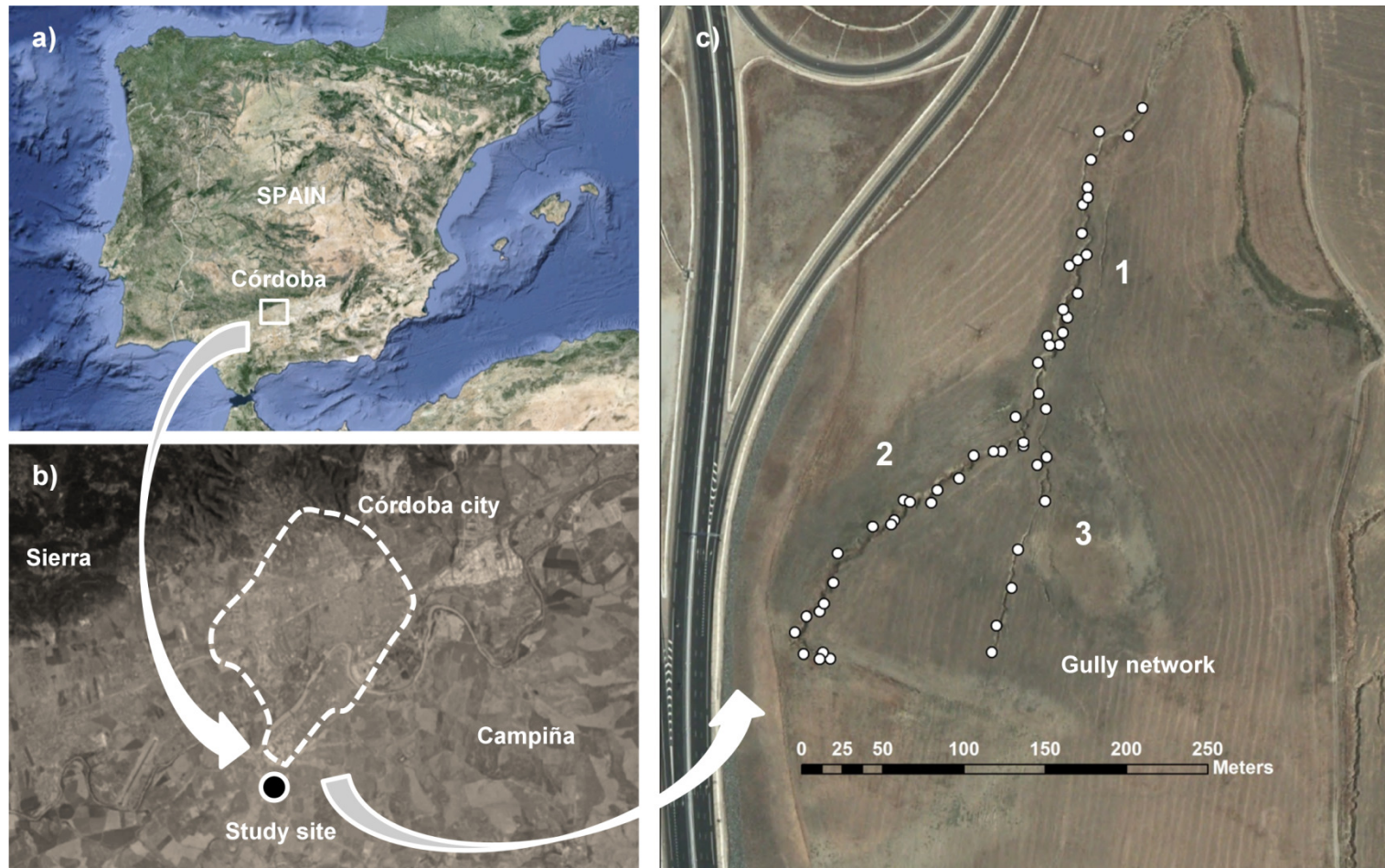
560

561



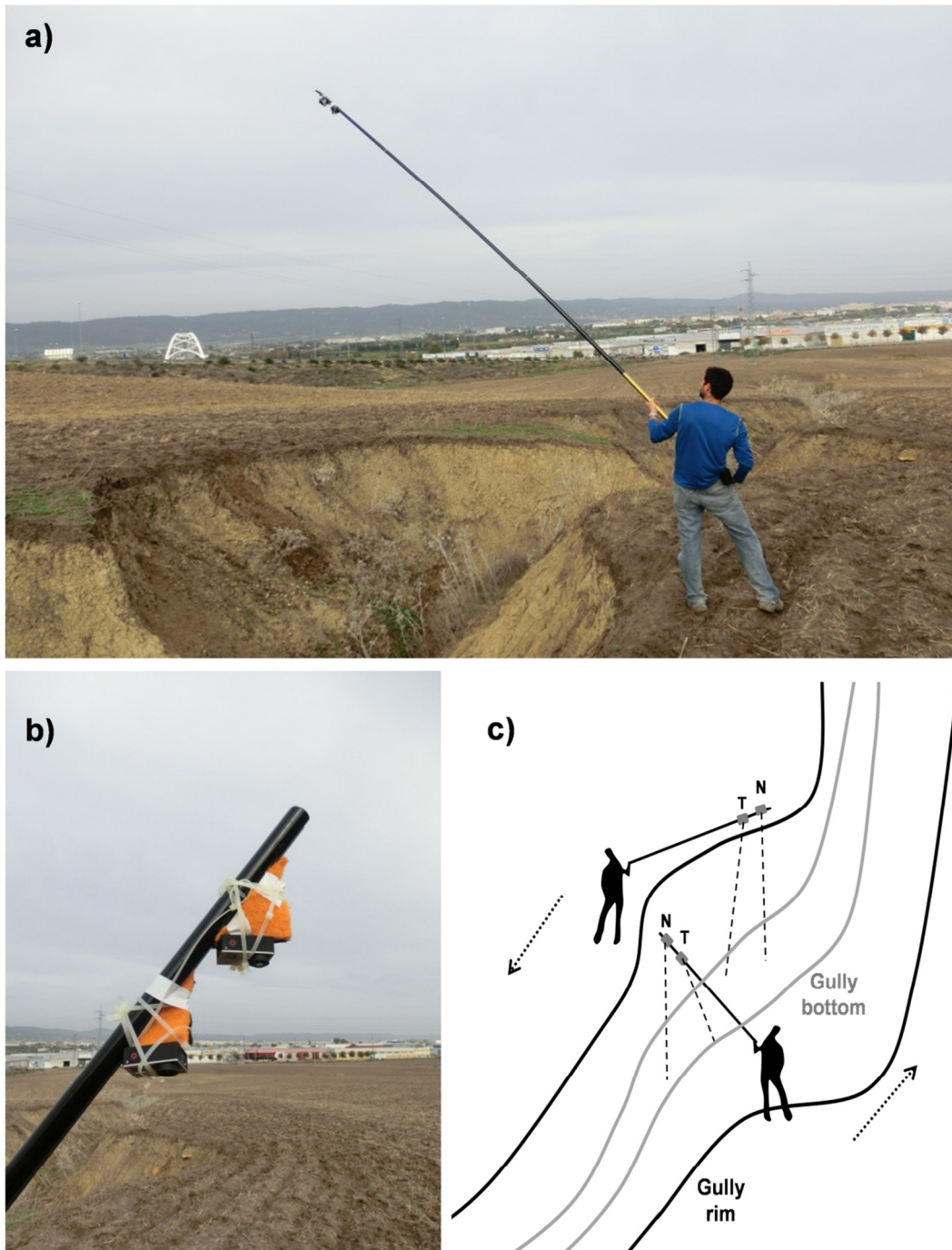
562

563 Figure 1. SF3M v1.0 with the main window on the right, image window on the upper-left and display window on the bottom-left. Among other
 564 SF3M features, the figure shows: 1) highlighting of image listbox with detected ground control points GCPs (yellow) and with observations
 565 (blue) in the observations window; 2) text in green colour for performed operations; 3) subproject listbox for subproject management; 4) GCPs
 566 table with mean georef and control errors. SF3M executable, license and instructions can be found at the SF3Mapp.csic.es domain.



567

568 Figure 2. a) and b) Location of the study site (source: <https://www.google.es/maps>); c) Plan view of the gully network with indication of the
 569 branch number for photo-reconstruction purposes from the 2011 orthophotography (Junta de Andalucía, 2015). In white dots, the location of the
 570 ground control points GCPs deployed in the gully.

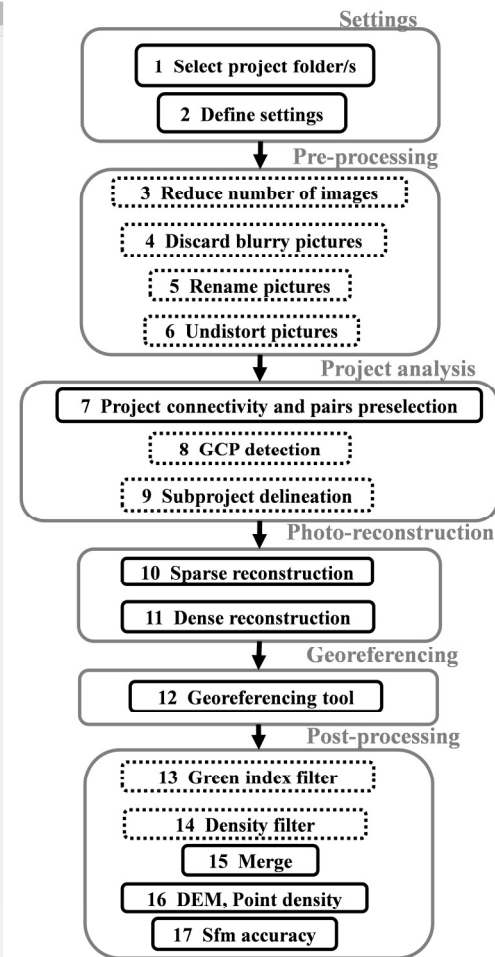
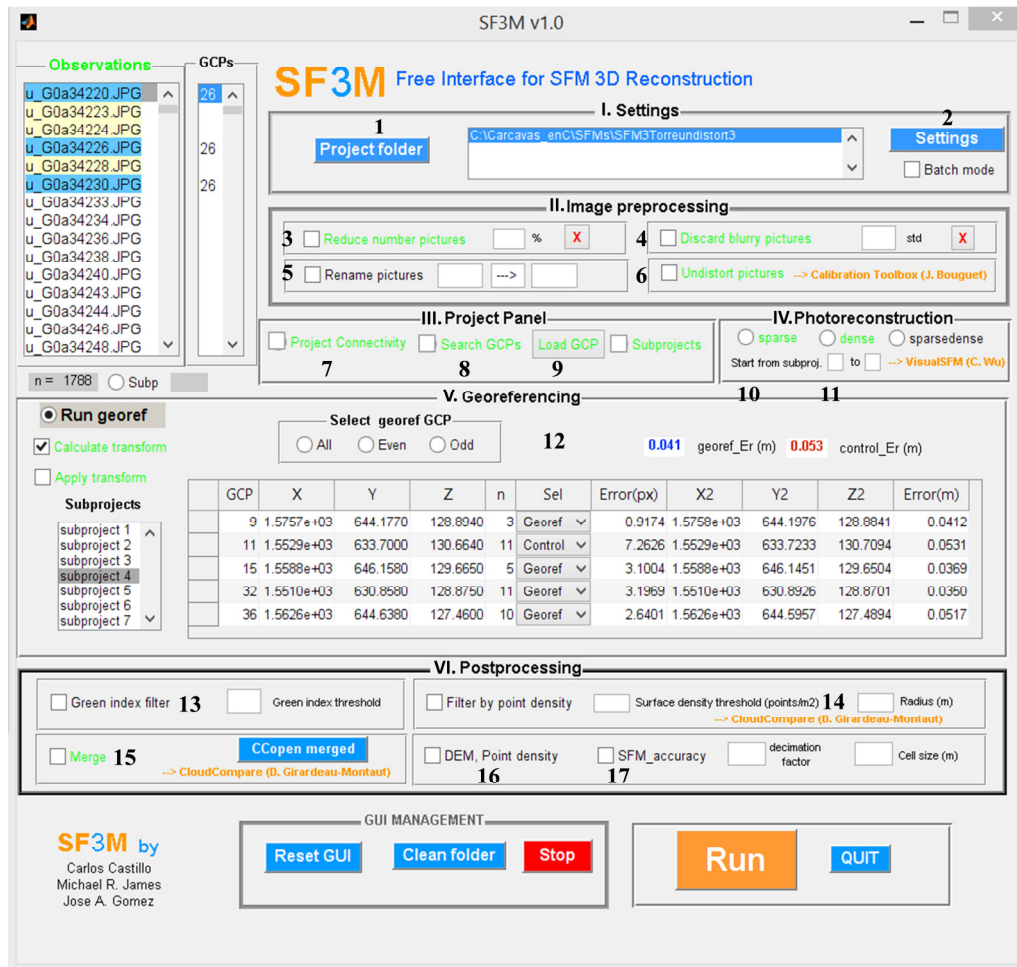


572

573 Figure 3. Camera operation in the gully erosion study: a) View of the operator during
 574 the field survey; b) Closer view of the two GoPro Hero3+ cameras on the 6 m pole with
 575 differential angle between cameras. c) Sketch of the image collection methodology as a
 576 walking itinerary along the gully perimeter. The rough nadir perspective (N)
 577 corresponds to the camera close to the pole tip and the tilted perspective (T) to the
 578 camera slightly below.

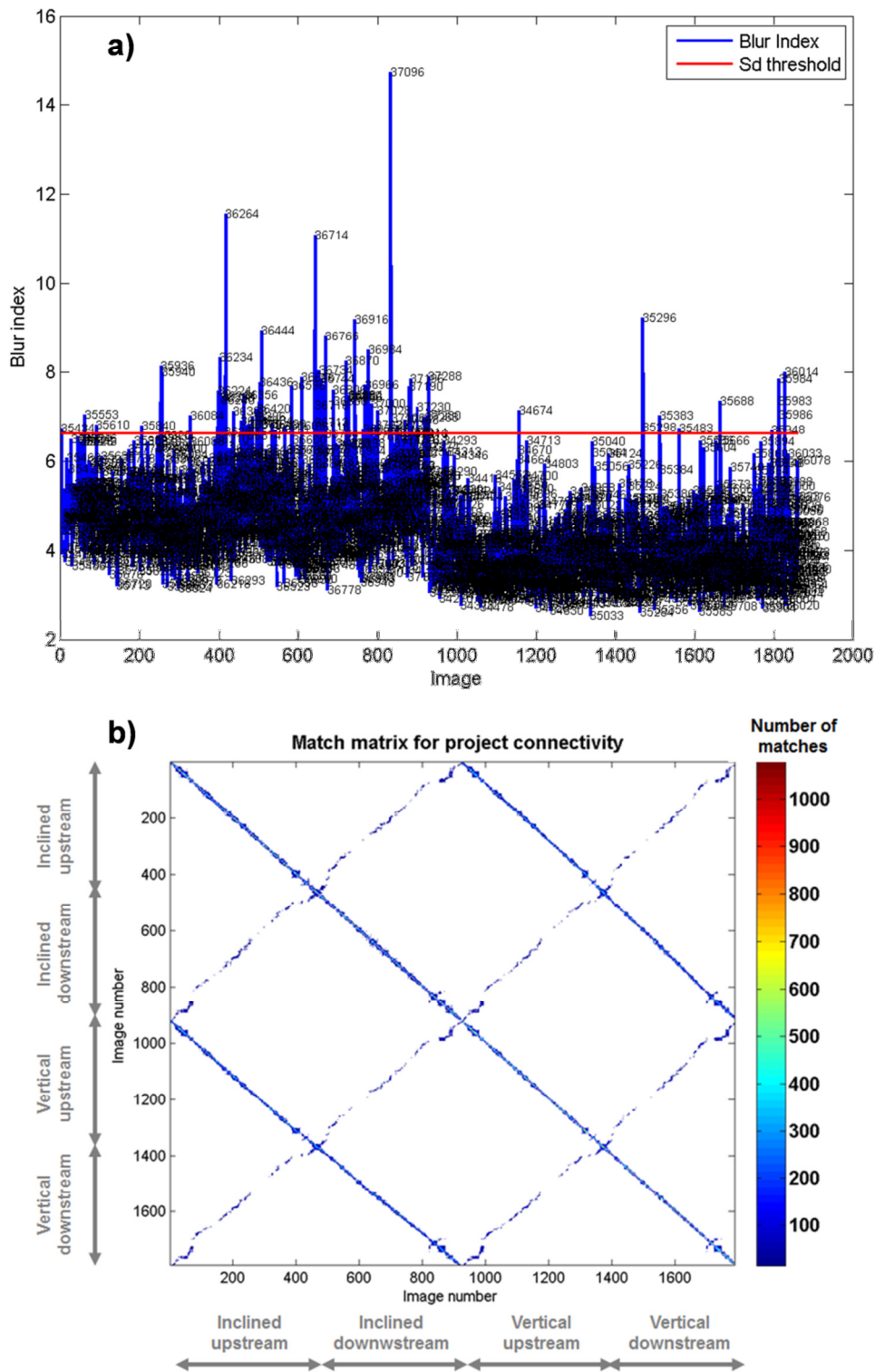
579

580



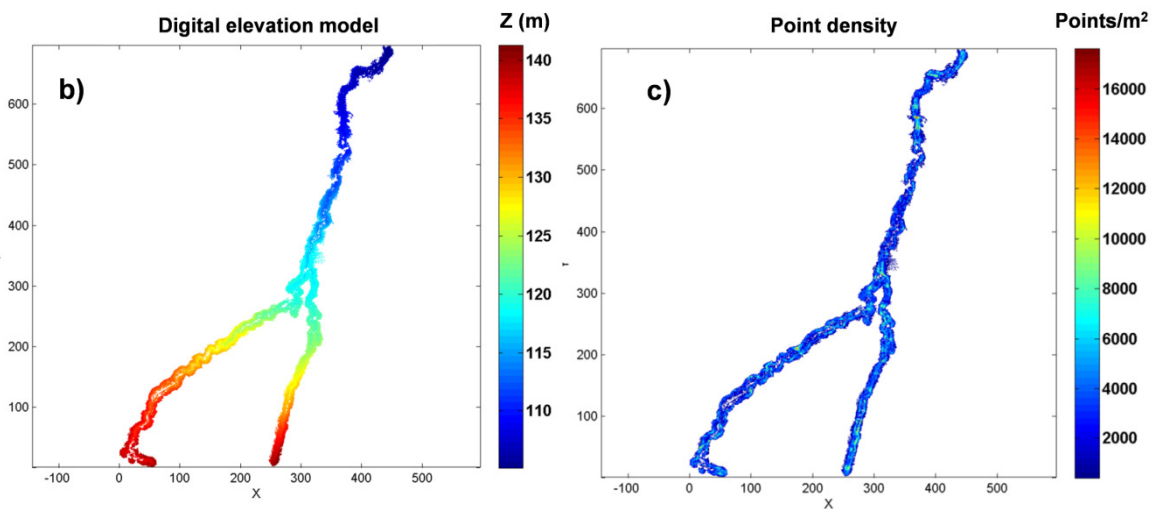
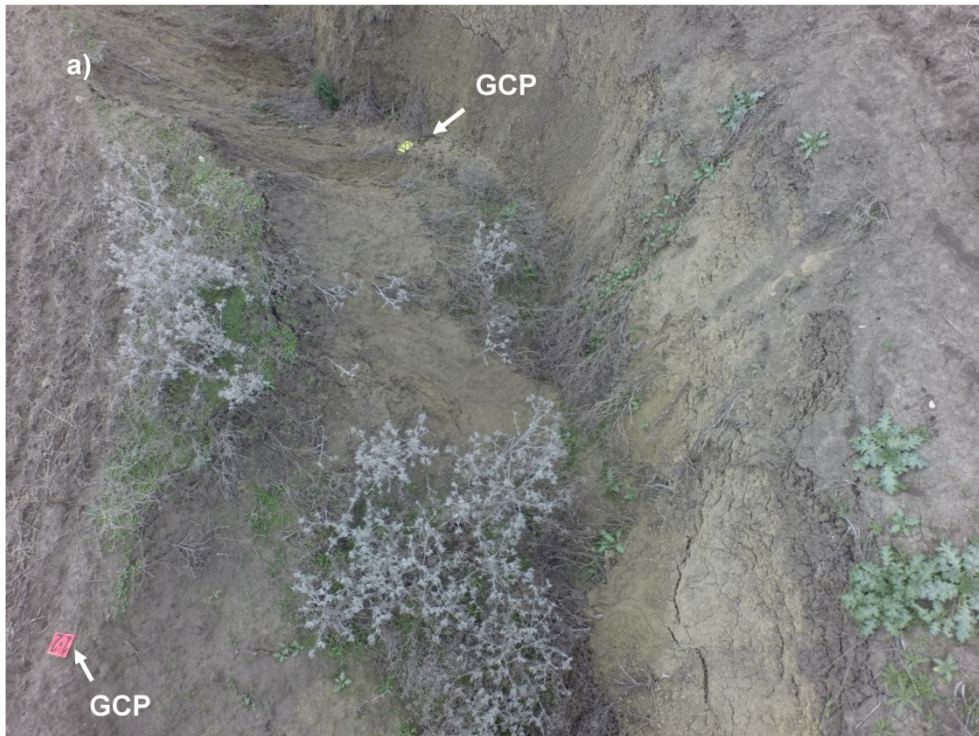
581

582 Figure 4. SF3M v1.0 workflow stages and their correspondence with command options on the SF3M main window. The dotted lines in the
583 diagram indicate optional stages in a reconstruction project.



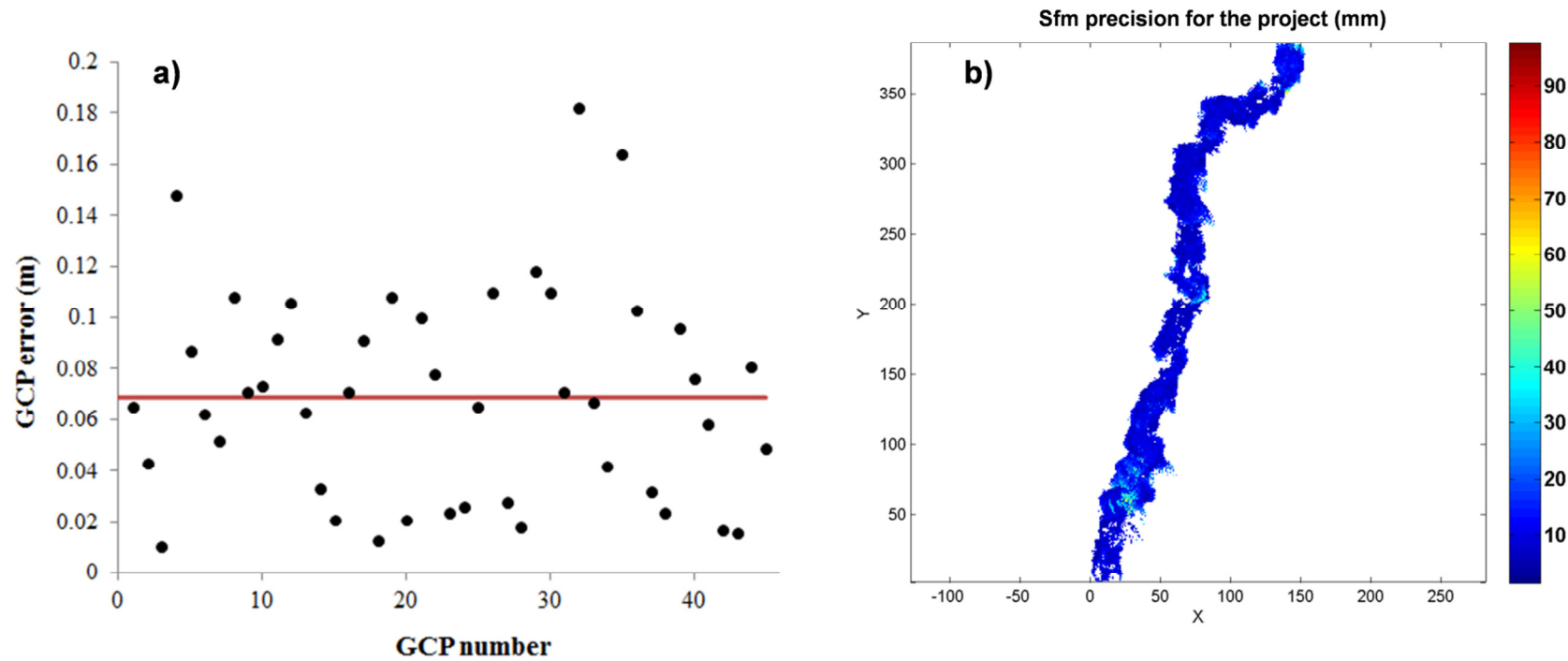
584

585 Figure 5. SF3M results of the pre-processing and project analysis stages for the gully
 586 branch 2: a) Blur index for the ~1800 image set with image number label. Those images
 587 outside the upper 2 standard deviations interval (red line) were discarded; b) matrix of
 588 matches with indication of the camera and direction in the image collection (in grey).
 589 The matrix of matches is symmetrical. Matches in the diagonal correspond to image sets
 590 only connected in the linear direction.



591

592 Figure 6. a) View of gully branch 2 from the inclined camera showing two ground
 593 control points GCPs; b) Digital elevation model (m) and c) point density map
 594 (points/m²) for the entire gully network from SF3M results. Several gaps in the 3D
 595 model can be noticed as a result of vegetation occlusion, mainly small green weeds
 596 (removed by the green index filter) and tall grey weeds (filtered by applying the point
 597 classification by CANUPO).



598

599 Figure 7. a) Error magnitudes on the 3D model (m) with dGPS ground control point measurements as the reference (the 0.069 m average in red
 600 line); b) Estimated SfM local precision in mm (Eq. 1) taking into account the residuals in the image measurements and the camera-point distance
 601 for gully branch 1. The dominant dark blue colours show that average precision is around 1-2 cm.

602

603

604



605

606 Figure 8. Views of the gully network in the 2007, 2009 and 2011 orthophotographies (Junta de Andalucía, 2015). Most probably, the gully was
607 landfilled in the summer of 2008 and, since then, there is no evidence of having been filled again.